Available online at www.sciencedirect.com

ScienceDirect

Focus Article, *Mendeleev Commun.*, 2018, **28**, 565–573

Mendeleev Communications

Nanoscale heterogeneities in ionic liquids: insights from EPR of spin probes

Mikhail Yu. Ivanov[a,b] and Matvey V. Fedin*[a,b]

[a] *International Tomography Center, Siberian Branch of the Russian Academy of Sciences, 630090 Novosibirsk, Russian Federation. E-mail: mfedin@tomo.nsc.ru*

[b] *Novosibirsk State University, 630090 Novosibirsk, Russian Federation*

DOI: 10.1016/j.mencom.2018.11.001

Self-organization is an important property of room-temperature ionic liquids (ILs). In particular, it gives rise to various heterogeneities occurring on the nanometer scale. However, the detection and characterization of such heterogeneities is often challenging, and the development of new experimental approaches for such studies is highly demanded. In this work we review recent progress in applications of electron paramagnetic resonance (EPR) to study heterogeneities in ILs over a broad temperature range. Since ILs are naturally diamagnetic, various spin probes and corresponding techniques have been used. We demonstrate that complex application of continuous wave, pulse and time-resolved EPR allows one to obtain unique information on formation and properties of heterogeneities in ILs, fruitfully complementing the data of other methods.

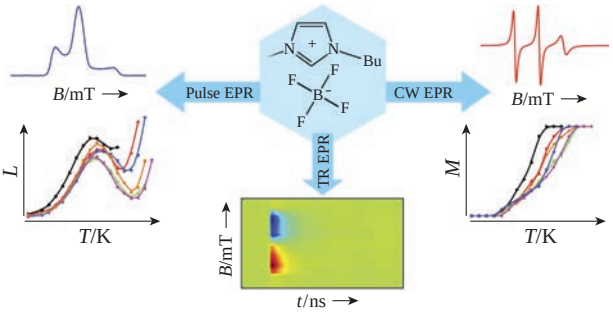

Introduction

Heterogeneities in ionic liquids (ILs) have been in focus of many experimental and theoretical studies over the past decade.[1–8] Apart from being a fundamentally important phenomenon, such heterogeneities have potential of being used in many practical applications including heterogeneous catalysis, drug delivery, new reaction pathways and chemical syntheses, *etc*. Because of that, the number of studies on heterogeneities and self-organization in ILs is rapidly growing.

ILs, also sometimes referred to as molten salts, are the mixtures of cations and anions which do not recombine into the solid state (see Figure 1 for examples). In many cases the cations/anions of different ILs are interchangeable, giving rise to a wide variety of compositions and properties, and opening up the way for high tunability of ILs for target applications.[9–20] Clearly, the structures and physicochemical properties of cations and anions are crucial for self-organization and formation of heterogeneities.[1–3,5,6,21–26] In particular, for most studied imidazolium-based ILs the heterogeneities occur due to the segregation of alkyl tails of cations in nonpolar nanodomains, as has been evidenced in a series of theoretical and experimental studies.[26–30] A lot of information on heterogeneities in ILs has been obtained using diffraction and scattering techniques.[7,8,24,28,31,32] Recently, nuclear magnetic

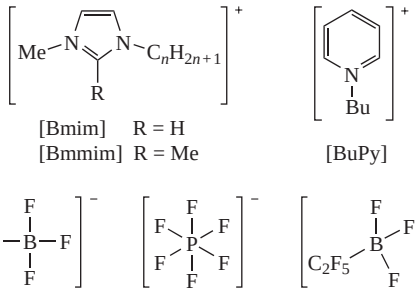

Figure 1 Representative structures of cations and anions forming ILs discussed.

Matvey V. Fedin is the head of Laboratory of Magnetic Resonance in International Tomography Center, Siberian Branch of the Russian Academy of Sciences. He received his PhD degree in chemical physics in 2002, Dr. Sci. degree in 2011, and became Professor of the Russian Academy of Sciences in 2016. His research interests include methodology and applications of electron paramagnetic resonance, with a special emphasis on topical and challenging systems of biology and materials science.

Mikhail Yu. Ivanov is a PhD Student of Physics Department in Novosibirsk State University. His research interests include application of EPR techniques in materials science, in particular, to study heterogeneities in ionic liquids, triplet systems with π-conjugation, electron-acceptor dyads. He also focuses on EPR instrumentation and microwave engineering.

resonance and cryoelectron microscopy have been applied to study heterogeneities in ILs on nano- and mesoscale, respectively.[5,25,29,33–37]

At the same time, full understanding of nature and physicochemical properties of such heterogeneities is far from being reached, and the growing variety of IL structures and applications needs more informative spectroscopic techniques to become available.[9,38–41] The use of electron paramagnetic resonance (EPR) spectroscopy to study ILs is noticeably different compared to other above-mentioned techniques. As a rule, ILs are diamagnetic and thus EPR-silent; therefore, an incorporation of special 'reporter' molecules, called spin probes, is necessary for EPR study.[42] This aspect has several definite pros and cons. On the one hand, when probe molecules are dissolved in neat IL, the specific solute–solvent interactions cannot be excluded. For instance, trace amounts of water (several tens ppm) are able to modify the network of hydrogen bonds in imidazolium-based ILs and noticeably alter their physical properties. Furthermore, if heterogeneities are formed, it is not generally clear whether they are natural for the studied IL or they are guest-induced. On the other hand, despite all said above, clearly, most of the imaginable applications of ILs will deal with guest molecules and thus necessarily include the solvent–solute interactions. Therefore, the use of probe-based techniques, such as EPR, might become very appropriate, especially if the probe molecules model the solutes in particular target application. Thus, it should be desirable to develop a series of probe molecules with different structural and physicochemical properties, along with the suitable experimental approaches yielding relevant information. Below we highlight some of the milestones achieved in this direction by us, as well as by other EPR spectroscopists.

EPR techniques

Since its discovery by Zavoisky in 1944,[43,44] EPR has become a widely used method of studying paramagnetic compounds. Most commonly, the continuous wave (CW) EPR is used.[45] In this 'basic' version of EPR, the microwave (mw) field is continuously applied to the sample, while the external magnetic field of spectrometer is being swept [Figures 2 and 3(*a*)]. When the energy of mw field $E_{mw} = h\nu$ matches the energy gap between two spin levels (where h is the Planck constant and ν is the mw frequency), the resonant absorption of mw energy can be detected, given that the matrix element of the corresponding transition is nonzero (see Figure 2). To enhance sensitivity of CW EPR, the magnetic field of spectrometer is usually modulated at kHz-range frequencies, and phase-sensitive detection is applied. As a result, the first derivative shapes of the absorption lines are experimentally detected.

Time-resolved (TR) EPR (often called transient EPR) is also a CW technique, where, most commonly, the timescale is initiated by a short (ns-range) laser pulse [Figure 3(*b*)].[46,47] The applied laser pulse can either lead to a formation of paramagnetic species from initially diamagnetic precursors, or it can change the spectroscopic properties of already existing paramagnetic species in the sample.[48,49] In any case, laser pulse induces the changes of the

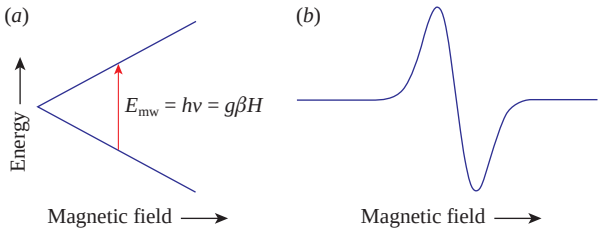

Figure 2 (*a*) Energy level diagram for the simplest spin system $S = 1/2$ with one electron and (*b*) a sketch of the corresponding EPR spectrum.

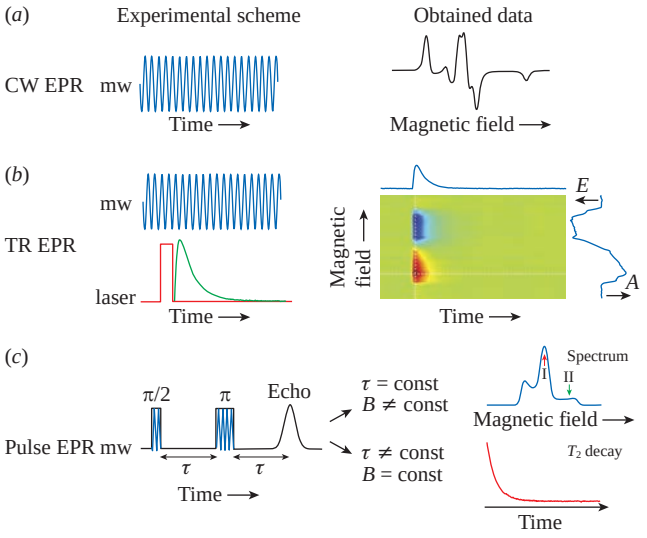

Figure 3 Principal schemes of (*a*) CW, (*b*) TR and (*c*) pulse EPR experiments. Examples of data that can be obtained using each method are given.

mw absorption, which can be monitored on nanosecond to submillisecond timescale as TR EPR kinetics. Generally, TR EPR kinetics has to be recorded in each magnetic field point within the spectral range of interest, so that the 2D data array is eventually obtained. Note, that magnetic field modulation is not used in TR EPR to avoid unwanted interference with the observed temporal processes. The sensitivity, as a rule, is recovered due to a high nonequilibrium spin polarization formed when TR EPR is applied to photochemical reactions or photoexcited triplet states.

Pulse EPR uses pulsed mw field instead of continuous irradiation [Figure 3(*c*)].[50,51] It comprises a large family of most informative EPR methods, which employ various pulse sequences and combinations of mw and radio-frequency fields. In most cases, an electron spin echo is detected, what can be done, *e.g.*, using the simplest Hahn echo sequence $\pi/2$–τ–π–τ–echo. Here $\pi/2$ and π refer to the mw pulses that rotate magnetization by angles $\pi/2$ and π, respectively, and τ is the interpulse delay. Variation of pulse lengths and interpulse delays constitutes temporal axis of pulse EPR methods and allows one to investigate dynamic and kinetic processes, as well as weak interactions in the spin systems.

Microscopic viscosity probed by CW EPR

Molecular-level organization of ILs has a lot of different manifestations and consequences; in particular, it leads to different physicochemical properties exhibited by ILs at micro- and macroscopic scale. For instance, this refers to the apparent values of viscosity obtained on the microscopic and macroscopic levels.

CW EPR of nitroxide probes (Figure 4) provides an elegant way to evaluate local viscosity of surrounding medium.[42,52] It is well known that the EPR spectrum of mobile nitroxide radical (*e.g.* in solutions or in soft amorphous media) is very sensitive to its rotational diffusion. This is nowadays broadly used in biological and materials science applications in order to probe local environment of radical or radical-labeled molecule.[53–59]

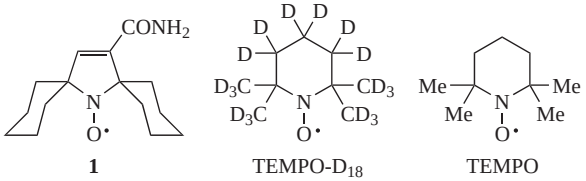

Figure 4 Examples of nitroxide spin probes used.

In particular, X-band (9 GHz) EPR allows precise measurement of the rotational correlation times of nitroxides in the range of ~0.1–10 ns to be made.[42,52] Figure 4 shows chemical structures of nitroxide **1**, TEMPO and TEMPO-D_{18} spin labels used in this study.

Many studies addressed the rotational dynamics of nitroxides in ILs probed by CW EPR.[60–68] In particular, it has been noticed that effective hydrodynamic radii obtained from rotational correlation times are much smaller than the expected ones, meaning that ILs are considerably less viscous at microscopic level than one would expect based on the macroscopic values of viscosity. This likely means that the radicals reside in micelle-like (cage-like) local environments providing smaller local viscosity. It was also found that polar substituent in nitroxide radical causes additional hydrogen bonding between the spin probes and ionic liquid.[61,63] Interestingly, the diffusion into the free volume of IL is a non-activated process, contrary to the case of common organic solvents.[62,69] Moreover, CW EPR has revealed interesting physics and chemistry of IL–water mixtures. The mesostructured aggregates with typical radii of ~120 nm and micelle-like structures were investigated, and correlations of such structures with water concentration and solvent temperature were established.[64,65,70]

The above studies were mainly focused on temperatures higher than the melting or glass transition points of corresponding ILs (T_m and T_g, respectively). In this way, they reflect the dynamic heterogeneities formed in liquid-state ILs at high temperatures, and the intermediate structures existing on sub-nanosecond timescale can be essentially averaged. At the same time, complementary insights into the nature of such heterogeneities can be obtained by 'snapshotting' of the structure. For instance, this can be done by shock-freezing the IL to form the IL glass. Note, that the same paradigm is broadly used in biological applications of EPR worldwide, as it is assumed that the structural states of complex biomolecules are essentially captured by shock-freezing in liquid nitrogen (77 K).[55,56,58,71] Therefore, it would also be desirable to derive information on local mobility of nitroxide probes in IL glasses and in the course of the glass/melting transitions.

Figure 5(*a*) shows CW EPR spectra of TEMPO-D_{18} radical dissolved in [Bmim]BF_4 in the temperature region well above the glass transition T_g. The spectral shapes noticeably depend on temperature reflecting the acceleration of radical rotation at higher *T*. Simulations yield values of rotational correlation times τ_c. Assuming diffusive rotational motion we can use Stokes–Einstein–Debye equation and known hydrodynamic radius of TEMPO (~0.34 nm)[72–74] to calculate the microviscosity sensed by the spin probe. Obtained correlation times indicate that the values of microscopic viscosity experienced by TEMPO-D_{18} change by roughly 2 orders of magnitude for all studied imidazolium-type ILs at T = 200−300 K and are by ~1–2 orders of magnitude smaller than the corresponding values of macroscopic viscosity.[75] We speculate that the huge difference between macroscopic and microscopic viscosities is due to the specific arrangement of solvent around the probe, originating from the structural organization of IL.

At temperatures close to the glass transition the rotational dynamics of spin probe changes in a principal manner, suggesting the coexistence of two different microenvironments surrounding radicals. To enhance spectral resolution and trace the formation of such heterogeneities, it is preferable to use spin probe with narrow EPR lines, such as deuterated TEMPO-D_{18} (see Figure 4). Figure 5(*b*) shows CW EPR spectra of TEMPO-D_{18} in [Bmim]BF_4 measured at several temperatures approaching and below T_g = = 187.7 K. Remarkably, experimental spectra at T ~ 170−270 K can only be simulated assuming superposition of two 'kinds' of spin probes. The first one refers to immobile nitroxides surrounded by solid-like medium [blue dotted line in Figure 5(*b*)]; the second

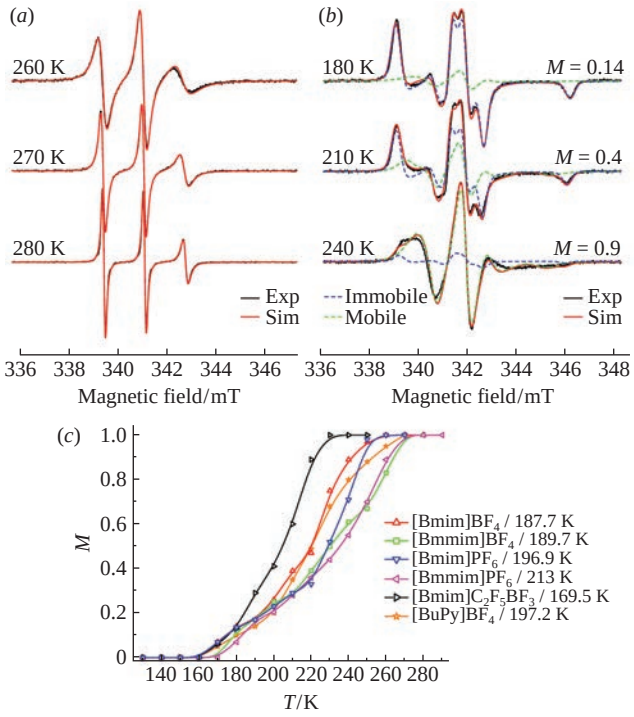

Figure 5 (*a*) Representative CW EPR spectra of TEMPO-D_{18} in [Bmim]BF_4 at $T > T_g$, T_m (Exp, black). Simulations (Sim) are shown in red; see ref. 76 for parameters. (*b*) Representative CW EPR spectra of TEMPO-D_{18} in [Bmim]BF_4 at T close to T_g (Exp, black). Best fits (Sim) are shown in red, contributions of mobile (M) and immobile ($1 - M$) fractions are shown in dotted green and blue, respectively; see ref. 76 for parameters. (*c*) Temperature dependence of the mobile fraction M in a series of ILs; see legend for IL structures and corresponding T_g values. Adapted from ref. 76.

one, instead, refers to mobile fraction dissolved in the liquid-like phase of IL [green dotted line in Figure 5(*b*)]. The latter undergoes slow rotational diffusion at low T and, as the temperature gets higher, gradually transforms into the fast motion regime, while the fraction of immobile nitroxides progressively vanishes. The relative fraction of each kind of spin probes *vs*. temperature can be obtained from the simulation, as is shown in Figure 5(*c*), where $M(T)$ is the relative fraction of mobile nitroxides. Note that such kind of spectral metamorphosis with coexistence of two nanoenvironments around spin probes is not typical of common organic solvents.[75] An important practical outcome of this finding is that by changing the temperature within *ca*. 160−260 K one can tune the ratio and the properties of local nanoenvironments in ILs, and in this way create new conditions for heterogeneous catalysis and other potential applications.

Local environments probed by TR EPR

As was already mentioned above, it is highly desirable to develop a set of EPR probes having different sizes, shapes, physicochemical properties in order to study heterogeneities in ILs in more detail. Nitroxides described in the previous section are rather small molecules; of course, they can be attached or incorporated into larger scaffolds, but then the rotational correlation time will likely exceed ~10 ns sensitivity limit, and information on the mobility will become unavailable anyway. For this sake, we considered several photoexcited triplet molecules in conjunction with TR EPR. The selected molecules of porphyrins and fullerenes families are much bigger than the nitroxides (Figure 6), and the timescale of TR EPR experiments and detectable processes typically extend from ~10 ns up to a few milliseconds. This implies there are good prerequisites that TR EPR of photoexcited triplet molecules dissolved in ILs can be a valuable complementary technique to probe nanoscale heterogeneities. Moreover, higher viscosity of ILs compared to many common solvents,

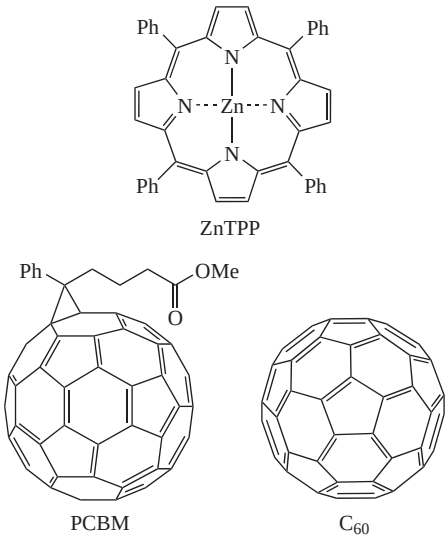

Figure 6 Structures of molecules, whose photoexcited triplet states were used as spin probes for TR EPR.

even at microscopic scale, might allow TR EPR on triplet molecules to be observed up to room temperatures. As a rule, triplet molecules have large intrinsic dipolar couplings (zero-field splittings), therefore fast rotational motion in liquid environment leads to a drastic shortening of the relaxation time and inability to detect TR EPR signal. Slowing down this rotation in ILs is expected to remedy this problem and make TR EPR studies possible in liquid state of IL as well.

Zn-tetraphenylporphyrin (ZnTPP, see Figure 6) is the known representative of triplet precursors yielding strong spin-polarized signals in TR EPR.[77–81] The TR EPR spectra of ZnTPP in ILs are principally similar to those in standard organic solvents. Figure 7 sketches the triplet energy levels, where the key parameters determining the spectral shapes are the zero-field splitting (ZFS) values.[82] In general, ZFS is contributed by dipole–dipole and spin–orbit interactions. It lifts the degeneracy of triplet levels in zero magnetic field ($|T_X\rangle$, $|T_Y\rangle$, $|T_Z\rangle$, molecular frame), and is characterized by two scalar parameters D and E,[47,83] whose physical meaning is illustrated in Figure 7. In disordered media, such as frozen solutions or powders, the resulting spectrum is a

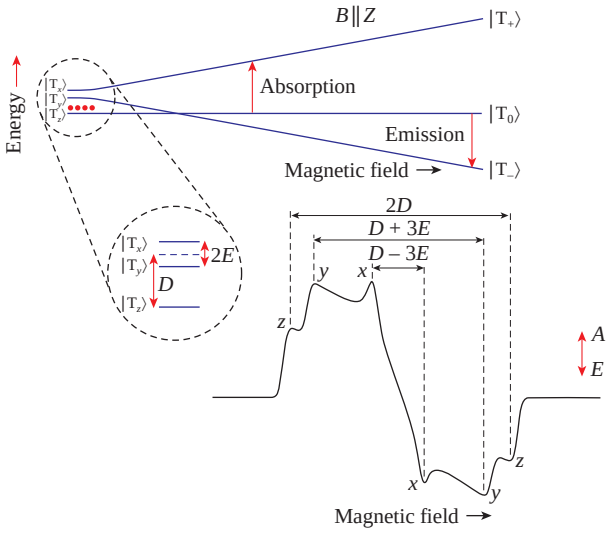

Figure 7 Energy level diagram of the triplet ($S = 1$) state for magnetic field B parallel to the Z axis of molecular frame; red arrows show the two EPR transitions. Levels structure in zero field is magnified, with representative nonequilibrium polarization depicted. Representative powder EPR spectrum for the polarization pattern shown in the top. Canonical orientations (x, y, z) are indicated, the corresponding energy differences in terms of D and E parameters are shown.

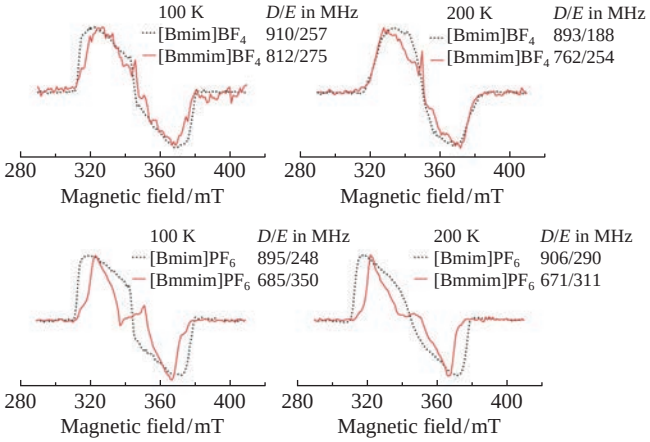

Figure 8 Experimental TR EPR spectra of ZnTPP in pairs [Bmim]BF_4, [Bmmim]BF_4 and [Bmim]PF_6, [Bmmim]PF_6; T = 100 and 200 K (adapted from ref. 84).

superposition of spectra of molecules having different orientation toward external magnetic field B. The characteristic spectral features arise at canonical orientations corresponding to B along the molecular axes X, Y, Z, with the splitting values determined by D and E (see Figure 7). The sign of the signal (spectrum phase) in each magnetic field can be either absorptive (A) or emissive (E) depending on the pattern of nonequilibrium populations of triplet levels. For example, Figure 7 illustrates the situation where zero-field $|T_Z\rangle$ state is predominantly populated. In high magnetic field this pattern yields enhanced populations of high-field state $|T_0\rangle$ (quantization onto direction of B) and results in absorptive low-field transition and emissive high-field transition. Thus, using computer simulations one can obtain both the ZFS parameters and the relative populations of triplet sublevels in photoexcited triplet molecules.

First of all, it is noteworthy that ZFS parameters D and E are different in different ILs. As an example, Figure 8 compares TR EPR spectra of ZnTPP in well-known imidazolium based ILs [Bmim]BF_4 and [Bmim]PF_6 with the spectra obtained in C2-methylated analogues of these ILs.[75,84]

The spectra in C2-methylated ILs (red in Figure 8) are narrower, and the canonical triplet peaks are sharper compared to C2-protonated ILs. Simulations show that the ZFS parameters of ZnTPP in C2-protonated ILs are close to those in other media found previously.[84] Contrary, in the case of C2-methylated ILs one clearly observes the trend of smaller D-values compared to those in other media, including C2-protonated analogs, and generally larger E-values (especially in case of [Bmmim]PF_6).[84] Since E relates to the rhombicity of the ZFS tensor and reflects the changes of molecular structure, we suggest that such a trend arises from the distortion of originally closely planar ZnTPP, supposedly due to the displacement of Zn atom out of the TPP plane and concomitant bending of the molecule. In general, correlations of D and E with the structure of IL should be studied in more detail in the future, since they might open additional opportunities to study solute–solvent interactions in ILs on a molecular level.

In contrast to CW EPR, TR EPR makes it possible to monitor the changes of the spectral shapes *vs.* time delay after laser flash (τ_{DAF}); in this way, information on spin and molecular dynamics of the paramagnetic reporter can be obtained (Figure 9). In particular, the detailed analysis of 2D TR EPR data on ZnTPP in ILs provides information on nanoenvironments surrounding the spin probe.

The shape of the TR EPR spectrum in ILs is explicitly contributed by two components, as is revealed by the changes in the spectrum shape *vs.* τ_{DAF} [Figure 9(*a*)]. The TR EPR spectrum

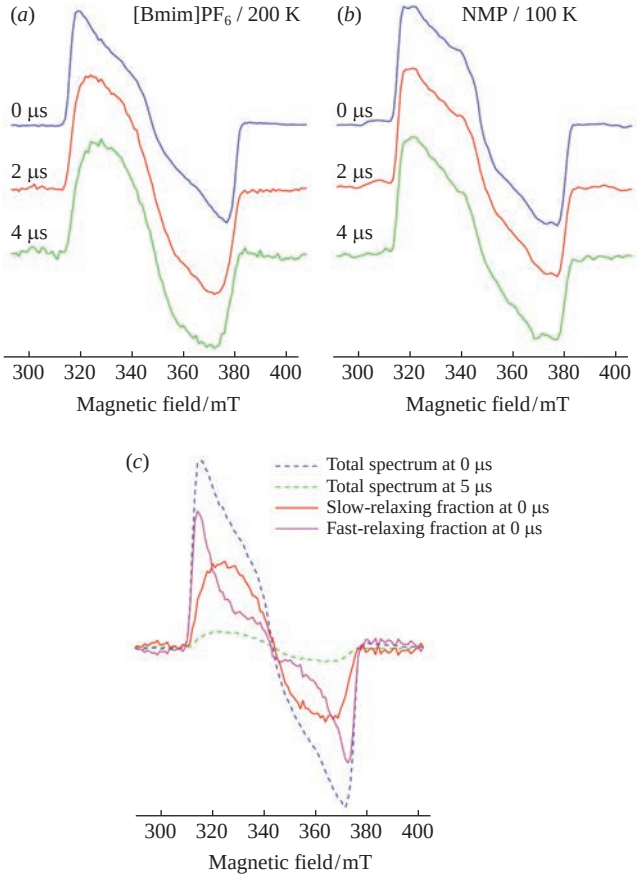

Figure 9 TR EPR spectra of ZnTPP *vs.* (τ_{DAF}) in (*a*) [Bmim]PF_6 and (*b*) common organic solvent *N*-methyl-2-pyrrolidone (NMP). (*c*) Illustrative decomposition of TR EPR spectrum in [Bmim]PF_6 into two components. Adapted from ref. 75.

of one component is characterized by relatively sharp peaks of canonical *Z*-orientations (B ~ 310 and 380 mT) and fast relaxation; therefore, its contribution is visible only at short τ_{DAF} [see Figure 9(*a*), 0 μs]. Such type of spectrum is similar to TR EPR spectra of ZnTPP observed in standard solvents [Figure 9(*b*)]. The second component has a more isotropic shape, resembling the TR EPR spectrum in liquid-state ILs, and relaxing much slower. The contributions of each spectral component can be disentangled [Figure 9(*c*)] using the decomposition procedure described in our previous work.[75] Briefly, this approach assumes coexistence of two fractions of ZnTPP having different relaxation rates, which, in turn, reflect different properties of surrounding environments. The relaxation rate of each component can be obtained from the simulation of TR EPR kinetic curve. Remarkably, no any significant variations of the TR EPR spectrum shape *vs.* τ_{DAF} were found for three common organic glasses [glycerol, toluene, and NMP presented in Figure 9(*b*)]. This supports the assignment of the observed variations of spectral shapes *vs.* time in ILs to a presence of two superimposed TR EPR spectra. In addition, we have found that spin polarization decays much slower in ILs compared to standard organic glasses. We explain this by a formation of molecular 'cages' (*e.g.*, micelle-like cavities of cationic alkyl tails) in frozen ILs, which agrees well with previous reported assumptions.[26,30,61,62,85] In this way, the slow-relaxing fraction is assigned to ZnTPP in such cavities, whereas the fast-relaxing fraction refers to ZnTPP in the frozen 'bulk' solvent. The molecules localized in the frozen bulk of IL show the relaxation behavior similar to that in common frozen solvents, whereas molecules inside the cavities of ILs exhibit slower relaxation. The slow-relaxing component in ILs is responsible for the overall long relaxation time compared to common organic solvents. This has an important practical implication meaning that polarization lifetimes of triplet molecules, when necessary, can be significantly increased by dissolving and studying them in ILs.

ZnTPP has a closely planar structure that can potentially lead to some specific interactions and motional modes. Therefore, triplet molecules of other shapes also need to be invoked to gain deeper understanding of the dimensions of micelle-like cavities in IL glasses.

Fullerenes are the suitable counterpart for this purpose and might have different sensitivity to local properties (in particular heterogeneities) of ILs compared to porphyrins, first of all due to their drastically different ball-like shapes.[86] In general, the solubility of fullerenes (*e.g.* C_{60}) in neat ILs is rather poor. This can be overcome in two ways: either by using alkyl-rich ILs (*e.g.* 1-decyl-3-methylimidazolium tetrafluoroborate, [C_{10}mim]BF_4) where the solubility increases, or by using fullerene derivatives with specific groups improving the solubility. We have selected two fullerenes to probe their sensitivities to heterogeneities and nanostructuring in ILs: C_{60} and its derivative PCBM (phenyl-C_{61}-butyric acid methyl ester, see Figure 6).

The low-temperature TR EPR spectrum of C_{60} in [C_{10}mim]BF_4 is noticeably different from that measured in common organic solvents, toluene and *o*-terphenyl, at similar T ~ 100 K (Figure 10). Well resolved perpendicular (x,y) and parallel (z) components of ZFS tensor are observed in IL [C_{10}mim]BF_4, whereas the spectra in common frozen solvents are virtually unresolved. It has been established earlier that C_{60} in glasses can undergo so-called pseudorotation, where Jahn–Teller-induced elongation of originally spherical molecule stochastically changes its direction.[87–91] Comparison of TR EPR spectra in [C_{10}mim]BF_4 and in common solvents indicates significant suppression of pseudorotation in IL. This assumption is supported by successful simulation of TR EPR spectrum of C_{60} in [C_{10}mim]BF_4 completely neglecting pseudorotation (see Figure 10).

The second fullerene probe PCBM (phenyl-C_{61}-butyric acid methyl ester) was chosen because of its better solubility in ILs compared to C_{60}, being due to additional functional butyric acid methyl ester group. The presence of this group lowers inherent symmetry of the fullerene molecule and potentially reduces the sensitivity of the probe to local environment. At the same time, lower symmetry results in significant suppression of pseudorotation. Indeed, TR EPR spectrum of PCBM exhibits well-resolved ZFS pattern even in common organic solvents, toluene

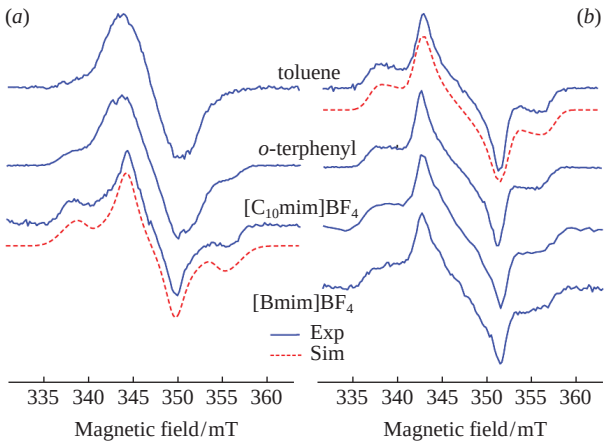

Figure 10 TR EPR spectra of (*a*) C_{60} and (*b*) PCBM measured at 90−100 K in various frozen solvents and ILs. All spectra were measured at time delays corresponding to the absorption maximum of the kinetics. The red curves show simulation. Adapted from ref. 86 (see this work for the simulation parameters).

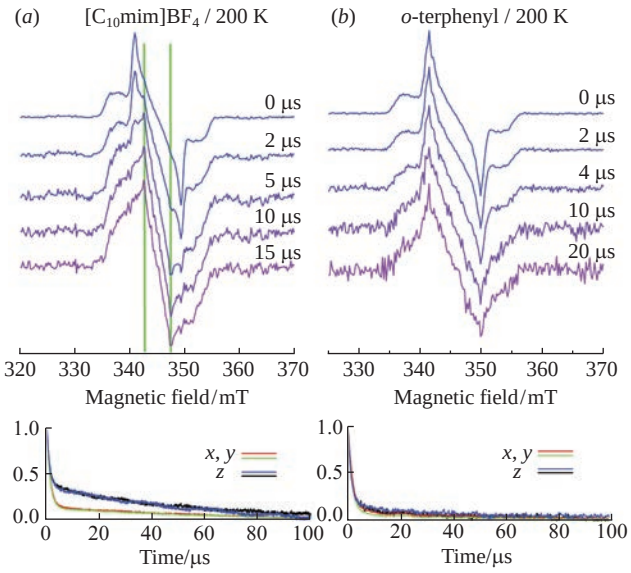

Figure 11 TR EPR spectra of PCBM measured at 200 K in (*a*) $[C_{10}mim]BF_4$ and (*b*) *o*-terphenyl. Time delays τ_{DAF} for TR EPR spectra are indicated for each trace. The green vertical lines for $[C_{10}mim]BF_4$ guide the eye for the transformation of spectral shape and peak positions. TR EPR kinetics are plotted below for (*x*,*y*) and *z* positions of both absorptive and emissive (inverted) parts of the spectrum. Adapted from ref. 86.

and *o*-terphenyl (see Figure 10), both due to the lowering of the symmetry and the lack of isotropic pseudorotation.

The fact that C_{60} is poorly soluble in $[Bmim]BF_4$ but can be dissolved in reasonable amounts in $[C_{10}mim]BF_4$ clearly emphasizes the role of longer alkyl chains of IL cation. Therefore, the dissolved C_{60} and PCBM molecules are likely localized in nonpolar micelle-like nanodomains of the segregated alkyl chains. If so, the rotational motion of a probe should be more intensive in ILs compared to common frozen solvents. Indeed, this is observed by in-depth analysis of 2D TR EPR data of PCBM in $[C_{10}mim]BF_4$ and in *o*-terphenyl (Figure 11). For example, TR EPR spectra in IL at 200 K manifest clear onset of a new spectral component, whose contribution grows with τ_{DAF} [Figure 11(*a*)] and is assigned to a more isotropic spectrum of a slowly rotating probe. Contrary, similar behavior is not found in common solvent [Figure 11(*b*)], and only becomes evident above T_m.

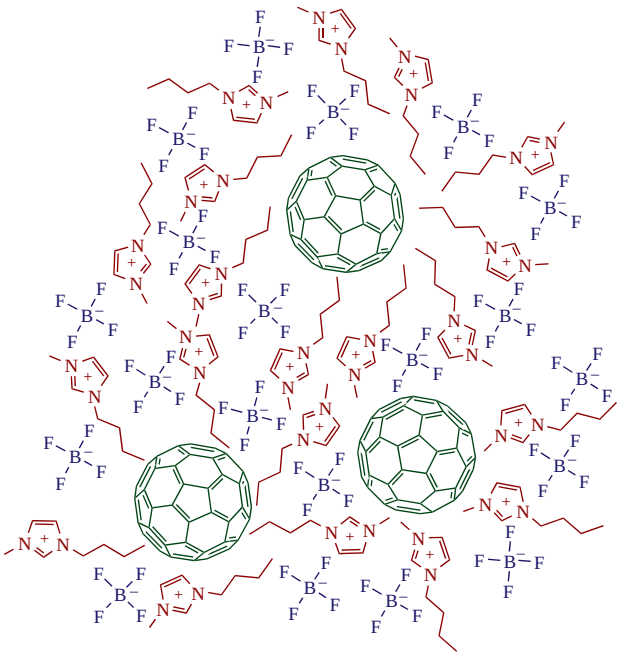

Figure 12 The sketch of partly ordered heterogeneous structure of IL with the dissolved fullerene probes.

The above TR EPR observations of the mobile fractions of photoexcited ZnTPP and PCBM in ILs near their T_g temperatures are coherent with CW EPR of nitroxide probes. This means that all three spin probes of drastically different size and geometry sense two local environments of IL, one of which promotes the molecular mobility and is likely a micelle-like environment. Based on this, we speculate that the sizes of such heterogeneities are at least comparable to the sizes of fullerene and porphyrin, being roughly 1 nm in diameter or the largest dimension (Figure 12).

Thus, TR EPR of photoexcited triplets provides several ways to reveal heterogeneities in ILs. In all cases, complex analysis of 2D TR EPR data is insightful. In case of porphyrin, the information stems from different mobilities of probes in different nanoenvironments. In addition, specific solute–solvent interactions manifest themselves in such spectroscopic parameters as zero-field splitting values. In case of fullerenes, pseudorotation or real diffusive motion of probe is sensitive to the local environments. Application of these approaches to imidazolium-based ILs indicates the presence of two local environments in IL glasses, one of which provides enhanced molecular mobility and likely originates from segregated alkyl chains of cations forming micelle-like nanostructures.

Heterogeneities probed by pulse EPR

CW and TR EPR methods yield important information on heterogeneities in ILs *via* the observation of large-scale motions (diffusive rotation) of the corresponding spin probes. However, as has been shown above, such motions arise at relatively high temperatures close to the glass transitions of ILs, whereas the lower-temperature regions with lower probe mobility remain unexplored. Here, the pulse EPR usefully complements the CW techniques. The molecules in glassy media are known to undergo the small-angle motions, often called stochastic molecular librations. In large series of works[92–94] a potent approach for characterization of stochastic librational motions in organic glasses and biopolymers using pulse EPR of embedded nitroxide probes was developed. Recently, we applied this approach for the first time to study molecular motions and local rigidity (stiffness) of ILs below and in the vicinity of their glass transitions.

Figure 3(*c*) shows a typical two-pulse echo-detected (ED) EPR spectrum of nitroxide obtained using Hahn's echo sequence $\pi/2$–τ–π–τ–echo. Due to the anisotropy of the hyperfine interaction between the unpaired electron and ^{14}N nucleus, the transverse relaxation time (T_2) turns out to be different at different magnetic field positions of the EPR spectrum. Therefore, a comparison of T_2 at two positions [marked as I and II in Figure 3(*c*)] allows one to characterize the mean-squared amplitude ($\langle\alpha^2\rangle$) and characteristic time (τ_c) of stochastic molecular libration motion. The experimentally obtained function $L(T) \equiv (1/T_2^{(II)} - 1/T_2^{(I)}) = 10^{11}\langle\alpha^2\rangle\tau_c$[76,93,95] *vs.* temperature is the most informative characteristic of stochastic molecular librations, where its onset and its slope characterize local rigidity/softness of the matrix surrounding spin probe.

We selected a set of ILs to probe experimentally local environments of the dissolved nitroxides using pulse EPR, namely $[Bmim]BF_4$, $[Bmim]PF_6$, $[Bmmim]BF_4$, $[Bmmim]PF_6$, $[C_{10}mim]BF_4$, $[Bmim]C_2F_5BF_3$, $[BuPy]BF_4$. For the comparison with common organic solvents, we performed measurements also in sucrose octaacetate (SOA), squalane, toluene and glycerol.[76,95] To allow pulse EPR measurements in the broader temperature range, it is beneficial to use the spirocyclohexane-substituted nitroxides (*e.g.* nitroxide **1**, see Figure 4) with advanced relaxation properties.

Figure 13 shows the obtained $L(T)$ dependencies in studied ILs, as well as in squalane and SOA. In case of ILs, each $L(T)$

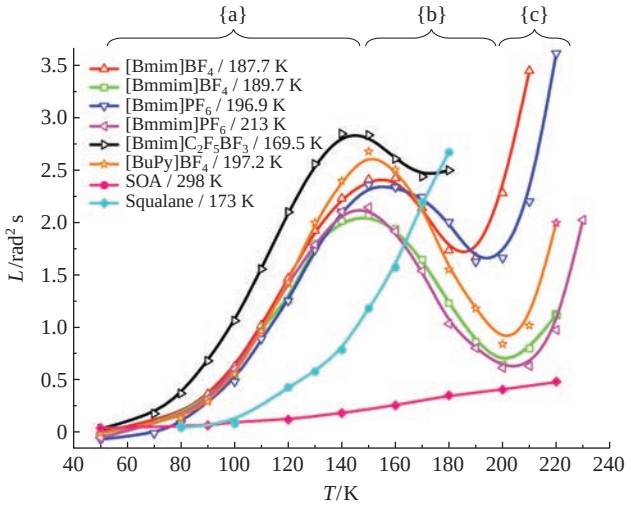

Figure 13 Temperature dependence of the motional parameter $L \approx 10^{11}\langle\alpha^2\rangle\tau_c$ for nitroxide radical **1** in ILs and in common organic glasses. The T_g for each compound is depicted in the legend; {a}, {b} and {c} indicate the motional regime, see text for details. Adapted from ref. 76.

curve shows three characteristic regions (marked {a}, {b} and {c}). The rise of $L(T)$ function at ~70 K (region {a}) indicates the onset of stochastic molecular librations in ILs at temperatures considerably lower than in common organic glasses squalane and SOA (> 100 K). Further increase of the stochastic librations amplitude [growth of $L(T)$] is observed up to ~140 K (region {a}). However, then the anomalous suppression of the stochastic librations is found within ~140−200 K (region {b}), which has never been observed in common organic glasses or biological membranes. At even higher temperatures T > 200 K, which are close to T_g of the studied ILs, the trend reverts to the rise again (region {c}), to be assigned to the unlocking of diffusive rotation of the radical in softened/melted IL.

The linear growth of $L(T)$ in region {a} is a typical behavior;[95] it was observed previously in various organic glasses and biological membranes.[96–98] Still, the comparative analysis of this temperature region allows one to draw certain conclusions on heterogeneities in ILs. In particular, within 80–150 K the stochastic librations appear to be consistently more intensive in ILs compared to common organic glasses (*e.g.* SOA or squalane, see Figure 13). The stochastic librations in glycerol and *o*-terphenyl are so weak within T = 80–150 K that they could not be detected at all. We explain considerably more intensive stochastic librations in frozen ILs by localization of nitroxides in the low-density nanodomains, most likely in nonpolar regions formed by segregated alkyl chains. In such 'micelle-like' environments the tumbling of nitroxide must be much less restricted. The additional support of this assignment is a great conformity of absolute values of $L(T)$ obtained in ILs and in biological membranes of unsaturated lipids.[98] Remarkably, the comparison with squalane clearly shows that more intensive stochastic librations in ILs are not solely due to abundance of surrounding alkyl chains, because local environment in ILs is even less dense than in the 'pure-chain' squalane. From general consideration, one reasonably expects that the robust manifestation of heterogeneities should occur when the dimensions of polar and nonpolar regions are comparable.

The nonlinear region {b} of $L(T)$ is rather interesting and unusual.[76] Most surprisingly, the drop of the $L(T)$ implies that the rigidity of local environment of nitroxide gradually increases with temperature between *ca.* 150 and 200 K. We propose that this anomaly can only occur due to specific structural rearrangements of ILs surrounding the nitroxide probe. Clear-cut correlations are found between the position of local minimum (on the border of regions {b} and {c}) and the T_g value of IL (see

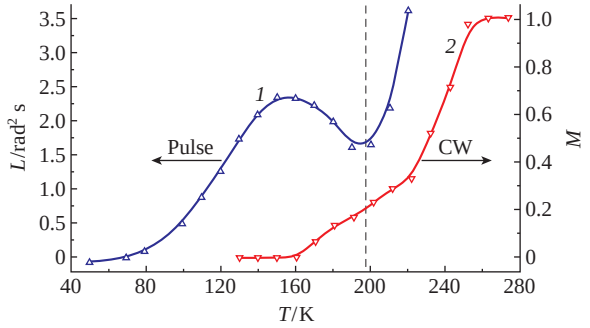

Figure 14 Temperature dependence of the (*1*) motional parameter $L \approx \approx 10^{11}\langle\alpha^2\rangle\tau_c$ and (*2*) mobile fraction M for [Bmim]PF_6. T_g is marked by a vertical dashed line. Adapted from ref. 76.

Figure 13 and T_g in the legends). Systematically, the unusual behavior occurs within ~40–60 K below the glass transition (this does not depend on the direction of the temperature change). To the best of our knowledge, such 'tightening' of local environment with temperature has never been observed in any solvent before. Remarkably, we have recently demonstrated that the observed anomaly is independent of the structure of spin probe,[99] and therefore is a true property of ionic liquid.

It is worth noting that the location of anomalous region {b} also correlates well with CW EPR data on mobile fraction of nitroxides (M), see above. Figure 14 shows the $L(T)$ function obtained by pulse EPR and $M(T)$ function obtained by CW EPR on the same plot (exemplified with the data of [Bmim]PF_6). One can notice that the onset of $M(T)$ occurs at $T \approx 160$ K and nearly coincides with the local maximum of $L(T)$, whereas the complete transition to a liquid phase occurs at around 270 K. CW EPR reveals the relative fraction of microenvironment where nitroxide exhibits slow diffusive rotation [$M(T)$], whereas this fraction becomes invisible for pulse EPR, because electron spin echo cannot be detected for a rotating nitroxide. At the same time, stochastic molecular librations detected by pulse EPR manifest themselves in another fraction of nitroxides [$1 - M(T)$], which appears 'immobile' in CW EPR. Thus, CW and pulse EPR fruitfully complement each other in the study of local environments and heterogeneities in ILs, and together they represent a versatile experimental approach.

Conclusions

Heterogeneities and molecular-level self-organization are the important properties of ILs, and their investigation using the dissolved probe molecules is very promising. In general, it provides information on the dimensions and nature of local nanoenvironments and solute–solvent interactions. In view of many potential applications of ILs, such local environments can eventually determine the routes of chemical and physical processes. In this review, we have demonstrated that the combination of CW, TR and pulse EPR techniques represents a versatile and extensive approach for investigation of heterogeneities in ILs. In particular, CW EPR detects the rotational motion of nitroxide spin probe and makes it possible to deduce the microviscosity values in liquid-state ILs. It also indicates the presence of different local environments of the probe at low temperatures, where the mobile and immobile fractions might coexist in a relatively broad temperature range. TR EPR of photoexcited triplet probes is even more sensitive to the heterogeneities in ILs. Such heterogeneities are identified by the analysis of TR EPR spectra *vs.* time, whose shape is highly sensitive to the molecular motion. Pulse EPR approach provides valuable information on small-angle molecular motions in IL glasses and allows one to make conclusions on the microscopic rigidity and local density of heterogeneities. The results of all three approaches converge

at assignment of the observed heterogeneities to the micelle-like cavities with the fraction of spin probes localized inside. Complex analysis of these EPR-derived data enables elucidation and comparison of such nanoenvironments sensed by solute molecules. Since tunable heterogeneities in ILs are of particular practical interest, the above methodology provides a promising tool for the future studies of nanoscale properties of ILs.

This work was supported by the Russian Science Foundation (grant no. 14-13-00826).

References

1 E. W. Castner, Jr., C. J. Margulis, M. Maroncelli and J. F. Wishart, *Annu. Rev. Phys. Chem*., 2011, **62**, 85.
2 P. Wasserscheid and W. Keim, *Angew. Chem. Int. Ed*., 2000, **39**, 3772.
3 K. E. Gutowski, G. A. Broker, H. D. Willauer, J. G. Huddleston, R. P. Swatloski, J. D. Holbrey and R. D. Rogers, *J. Am. Chem. Soc*., 2003, **125**, 6632.
4 A. Mele, C. D. Tran and S. H. de Paoli Lacerda, *Angew. Chem. Int. Ed*., 2003, **42**, 4364.
5 A. S. Kashin, K. I. Galkin, E. A. Khokhlova and V. P. Ananikov, *Angew. Chem. Int. Ed*., 2016, **55**, 2161.
6 Y. Wang and G. A. Voth, *J. Am. Chem. Soc*., 2005, **127**, 12192.
7 O. Russina, A. Triolo, L. Gontrani and R. Caminiti, *J. Phys. Chem. Lett*., 2012, **3**, 27.
8 O. Russina and A. Triolo, *Faraday Discuss*., 2012, **154**, 97.
9 H. Weingärtner, *Angew. Chem. Int. Ed*., 2008, **47**, 654.
10 T. L. Greaves and C. J. Drummond, *Chem. Rev*., 2015, **115**, 11379.
11 K. S. Egorova, E. G. Gordeev and V. P. Ananikov, *Chem. Rev*., 2017, **117**, 7132.
12 M. Zhang, R. Ettelaie, T. Yan, S. Zhang, F. Cheng, B. P. Binks and H. Yang, *J. Am. Chem. Soc*., 2017, **139**, 17387.
13 M. Blesic, M. H. Marques, N. V. Plechkova, K. R. Seddon, L. P. N. Rebelo and A. Lopes, *Green Chem*., 2007, **9**, 481.
14 D. Zhao, M. Wu, Y. Kou and E. Min, *Catal. Today*, 2002, **74**, 157.
15 M. L. Pusey, M. S. Paley, M. B. Turner and R. D. Rogers, *Cryst. Growth Des*., 2007, **7**, 787.
16 S. V. Savilov, A. O. Artemova, A. S. Ivanov, Z. Shen, S. M. Aldoshin and V. V. Lunin, *Mendeleev Commun*., 2016, **26**, 240.
17 A. S. Kucherenko, V. V. Perepelkin, G. M. Zhdankina, G. V. Kryshtal, E. Srinivasan, H. Inani and S. G. Zlotin, *Mendeleev Commun*., 2016, **26**, 388.
18 S. V. Kochetkov, A. S. Kucherenko and S. G. Zlotin, *Mendeleev Commun*., 2017, **27**, 473.
19 V. G. Krasovskiy, E. A. Chernikova, L. M. Glukhov, E. A. Redina, G. I. Kapustin, A. A. Koroteev and L. M. Kustov, *Mendeleev Commun*., 2017, **27**, 605.
20 M. G. Chernysheva, A. E. Averina, O. A. Soboleva and G. A. Badun, *Mendeleev Commun*., 2017, **27**, 296.
21 M. Wakasa, *J. Phys. Chem. B*, 2007, **111**, 9434.
22 R. Hayes, G. G. Warr and R. Atkin, *Chem. Rev*., 2015, **115**, 6357.
23 J. N. A. Canongia Lopes and A. A. H. Pádua, *J. Phys. Chem. B*, 2006, **110**, 3330.
24 C. S. Santos, H. V. R. Annapureddy, N. S. Murthy, H. K. Kashyap, E. W. Castner, Jr. and C. J. Margulis, *J. Chem. Phys*., 2011, **134**, 064501, DOI 10.1063/1.3526958.
25 M. M. Seitkalieva, A. A. Grachev, K. S. Egorova and V. P. Ananikov, *Tetrahedron*, 2014, **70**, 6075.
26 Y. Ji, R. Shi, Y. Wang and G. Saielli, *J. Phys. Chem. B*, 2013, **117**, 1104.
27 T. L. Greaves and C. J. Drummond, *Chem. Soc. Rev*., 2013, **42**, 1096.
28 A. Triolo, O. Russina, H.-J. Bleif and E. Di Cola, *J. Phys. Chem. B*, 2007, **111**, 4641.
29 A. E. Khudozhitkov, P. Stange, B. Golub, D. Paschek, A. G. Stepanov, D. I. Kolokolov and R. Ludwig, *Angew. Chem. Int. Ed*., 2017, **56**, 14310.
30 S. M. Urahata and M. C. C. Ribeiro, *J. Phys. Chem. Lett*., 2010, **1**, 1738.
31 A. Triolo, A. Mandanici, O. Russina, V. Rodriguez-Mora, M. Cutroni, C. Hardacre, M. Nieuwenhuyzen, H.-J. Bleif, L. Keller and M. A. Ramos, *J. Phys. Chem. B*, 2006, **110**, 21357.
32 R. Hayes, S. Imberti, G. G. Warr and R. Atkin, *Phys. Chem. Chem. Phys*., 2011, **13**, 3237.
33 M.-A. Sani, P.-A. Martin, R. Yunis, F. Chen, M. Forsyth, M. Deschamps and L. A. O'Dell, *J. Phys. Chem. Lett*., 2018, **9**, 1007.
34 A. C. Forse, J. M. Griffin, C. Merlet, P. M. Bayley, H. Wang, P. Simon and C. P. Grey, *J. Am. Chem. Soc*., 2015, **137**, 7231.
35 H. K. Stassen, R. Ludwig, A. Wulf and J. Dupont, *Chem. Eur. J*., 2015, **21**, 8324.
36 S. Cha, M. Ao, W. Sung, B. Moon, B. Ahlström, P. Johansson, Y. Ouchi and D. Kim, *Phys. Chem. Chem. Phys*., 2014, **16**, 9591.
37 A. E. Khudozhitkov, P. Stange, A.-M. Bonsa, V. Overbeck, A. Appelhagen, A. G. Stepanov, D. I. Kolokolov, D. Paschek and R. Ludwig, *Chem. Commun*., 2018, **54**, 3098.
38 N. E. Heimer, R. E. Del Sesto, Z. Meng, J. S. Wilkes and W. R. Carper, *J. Mol. Liq*., 2006, **124**, 84.
39 S. P. Ong, O. Andreussi, Y. Wu, N. Marzari and G. Ceder, *Chem. Mater*., 2014, **23**, 1.
40 H. Watanabe, H. Doi, S. Saito, M. Matsugami, K. Fujii, R. Kanzaki, Y. Kameda and Y. Umebayashi, *J. Mol. Liq*., 2016, **217**, 35.
41 V. H. Paschoal, L. F. O. Faria and M. C. C. Ribeiro, *Chem. Rev*., 2017, **117**, 7053.
42 E. Bordignon, *eMagRes*, 2017, **6**, 235.
43 E. K. Zavoisky, *Zh. Eksp. Teor. Fiz*., 1945, **15**, 344 (in Russian).
44 E. K. Zavoisky, *J. Phys.*, 1945, **9**, 211.
45 A. Van Der Est, *eMagRes*, 2016, **5**, 1411.
46 M. D. E. Forbes, L. E. Jarocha, S. Sim and V. F. Tarasov, in *Advances in Physical Organic Chemistry*, eds. I. Williams and N. Williams, Elsevier, 2013, vol. 47, ch. 1, pp. 1–83.
47 S. Weber, *eMagRes*, 2017, **6**, 255.
48 I. Yu. Barskaya, E. V. Tretyakov, R. Z. Sagdeev, V. I. Ovcharenko, E. G. Bagryanskaya, K. Yu. Maryunina, T. Takui, K. Sato and M. V. Fedin, *J. Am. Chem. Soc*., 2014, **136**, 10132.
49 M. V. Fedin, E. G. Bagryanskaya, H. Matsuoka, S. Yamauchi, S. L. Veber, K. Yu. Maryunina, E. V. Tretyakov, V. I. Ovcharenko and R. Z. Sagdeev, *J. Am. Chem. Soc*., 2012, **134**, 16319.
50 A. Schweiger and G. Jeschke, *Principles of Pulse Electron Paramagnetic Resonance*, Oxford University Press, Oxford, 2001.
51 S. Stoll, *eMagRes*, 2017, **6**, 23.
52 D. J. Schneider and J. H. Freed, in *Biological Magnetic Resonance*, eds. L. J. Berliner and J. Reuben, Springer, Boston, 1989, pp. 1–76.
53 M. Gränz, N. Erlenbach, P. Spindler, D. B. Gophane, L. S. Stelzl, S. T. Sigurdsson and T. F. Prisner, *Angew. Chem. Int. Ed*., 2018, **57**, 10540.
54 E. Bordignon and S. Bleicken, *Biochim. Biophys. Acta – Biomembr*., 2018, **1860**, 841.
55 S. Van Doorslaer, *J. Magn. Reson*., 2017, **280**, 79.
56 H. S. McHaourab, P. R. Steed and K. Kazmier, *Structure*, 2011, **19**, 1549.
57 V. Meyer, M. A. Swanson, L. J. Clouston, P. J. Boratyński, R. A. Stein, H. S. Mchaourab, A. Rajca, S. S. Eaton and G. R. Eaton, *Biophys. J*., 2015, **108**, 1213.
58 T. Maly, K. Zwicker, A. Cernescu, U. Brandt and T. F. Prisner, *Biochim. Biophys. Acta – Bioenerg*., 2009, **1787**, 584.
59 P. Zou, M. Bortolus and H. S. Mchaourab, *J. Mol. Biol*., 2009, **393**, 586.
60 Y. Akdogan, J. Heller, H. Zimmermann and D. Hinderberger, *Phys. Chem. Chem. Phys*., 2010, **12**, 7874.
61 R. Stoesser, W. Herrmann, A. Zehl, V. Strehmel and A. Laschewsky, *ChemPhysChem*, 2006, **7**, 1106.
62 R. Stoesser, W. Herrmann, A. Zehl, A. Laschewsky and V. Strehmel, *Z. Phys. Chem*., 2006, **220**, 1309.
63 V. Strehmel, *ChemPhysChem*, 2012, **13**, 1649.
64 D. R. Kattnig, Y. Akdogan, I. Lieberwirth and D. Hinderberger, *Mol. Phys*., 2013, **111**, 2723.
65 D. R. Kattnig and D. Hinderberger, *Chem. Asian J*., 2012, **7**, 1000.
66 B. Y. Mladenova, N. A. Chumakova, V. I. Pergushov, A. I. Kokorin, G. Grampp and D. R. Kattnig, *J. Phys. Chem. B*, 2012, **116**, 12295.
67 N. A. Chumakova, V. I. Pergushov, A. Kh. Vorobiev and A. I. Kokorin, *Appl. Magn. Reson*., 2010, **39**, 409.
68 B. Y. Mladenova, D. R. Kattnig and G. Grampp, *J. Phys. Chem. B*, 2011, **115**, 8183.
69 V. Strehmel, A. Laschewsky, R. Stoesser, A. Zehl and W. Herrmann, *J. Phys. Org. Chem*., 2006, **19**, 318.
70 D. R. Kattnig, Y. Akdogan, C. Bauer and D. Hinderberger, *Z. Phys. Chem*., 2012, **226**, 1363.
71 E. R. Georgieva, A. S. Roy, V. M. Grigoryants, P. P. Borbat, K. A. Earle, C. P. Scholes and J. H. Freed, *J. Magn. Reson*., 2012, **216**, 69.
72 L. Andreozzi, F. Cianflone, C. Donati and D. Leporini, *J. Phys. Condens. Matter*, 1996, **8**, 3795.
73 L. Andreozzi, A. Di Schino, M. Giordano and D. Leporini, *Europhys. Lett*., 1997, **38**, 669.

74 I. Peric, D. Merunka, B. L. Bales and M. Peric, *J. Phys. Chem. Lett.*, 2013, **4**, 508.
75 M. Yu. Ivanov, S. L. Veber, S. A. Prikhod'ko, N. Yu. Adonin, E. G. Bagryanskaya and M. V. Fedin, *J. Phys. Chem. B*, 2015, **119**, 13440.
76 M. Yu. Ivanov, S. A. Prikhod'ko, N. Yu. Adonin, I. A. Kirilyuk, S. V. Adichtchev, N. V. Surovtsev, S. A. Dzuba and M. V. Fedin, *J. Phys. Chem. Lett.*, 2018, **9**, 4607.
77 H. Levanon, *Chem. Phys. Lett.*, 1982, **90**, 465.
78 H. Aota, Y. Morishima and M. Kamachi, *Photochem. Photobiol.*, 1993, **57**, 989.
79 Y. Morishima, K. Saegusa and M. Kamachi, *J. Phys. Chem.*, 1995, **99**, 4512.
80 K. Ishii, T. Ishizaki and N. Kobayashi, *Appl. Magn. Reson.*, 2003, **23**, 369.
81 S. Yamauchi, K. Takahashi, S. S. M. Islam, Y. Ohba and V. Tarasov, *J. Phys. Chem. B*, 2010, **114**, 14559.
82 J. Telser, *eMagRes*, 2017, **6**, 207.
83 A. Carrington and A. D. McLachlan, *Introduction to Magnetic Resonance with Applications to Chemistry and Chemical Physics*, Harper and Row, New York, 1967.
84 M. Yu. Ivanov, S. A. Prikhod'ko, N. Yu. Adonin, E. G. Bagryanskaya and M. V. Fedin, *Z. Phys. Chem.*, 2017, **231**, 391.
85 B. Rotenberg and M. Salanne, *J. Phys. Chem. Lett.*, 2015, **6**, 4978.
86 I. V. Kurganskii, M. Yu. Ivanov and M. V. Fedin, *J. Phys. Chem. B*, 2018, **122**, 6815.
87 G. L. Closs, P. Gautam, D. Zhang, P. J. Krusic, S. A. Hill and E. Wasserman, *J. Phys. Chem.*, 1992, **96**, 5228.
88 M. Terazima, K. Sakurada, N. Hirota, H. Shinohara and Y. Saito, *J. Phys. Chem.*, 1993, **97**, 5447.
89 M. Bennati, A. Grupp and M. Mehring, *J. Chem. Phys.*, 1995, **102**, 9457.
90 S. Ceola, L. Franco and C. Corvaja, *J. Phys. Chem. B*, 2004, **108**, 9491.
91 M. N. Uvarov, L. V. Kulik, M. A. Bizin, V. N. Ivanova, R. B. Zaripov and S. A. Dzuba, *J. Phys. Chem. A*, 2008, **112**, 2519.
92 S. A. Dzuba, *Spectrochim. Acta, Part A*, 2000, **56**, 227.
93 N. P. Isaev and S. A. Dzuba, *J. Phys. Chem. B*, 2008, **112**, 13285.
94 D. A. Erilov, R. Bartucci, R. Guzzi, D. Marsh, S. A. Dzuba and L. Sportelli, *Biophys. J.*, 2004, **87**, 3873.
95 M. Yu. Ivanov, O. A. Krumkacheva, S. A. Dzuba and M. V. Fedin, *Phys. Chem. Chem. Phys.*, 2017, **19**, 26158.
96 S. V. Paschenko, Yu. V. Toropov, S. A. Dzuba, Yu. D. Tsvetkov and A. K. Vorobiev, *J. Chem. Phys.*, 1999, **110**, 8150.
97 R. Bartucci, R. Guzzi, M. De Zotti, C. Toniolo, L. Sportelli and D. Marsh, *Biophys. J.*, 2008, **94**, 2698.
98 V. N. Syryamina and S. A. Dzuba, *J. Phys. Chem. B*, 2017, **121**, 1026.
99 A. A. Kuzhelev, O. A. Krumkacheva, M. Yu. Ivanov, S. A. Prikhod'ko, N. Yu. Adonin, V. M. Tormyshev, M. K. Bowman, M. V. Fedin and E. G. Bagryanskaya, *J. Phys. Chem. B*, 2018, **122**, 8624.

Received: 29th August 2018; Com. 18/5676